

A novel layer-structured scaffold with large pore sizes suitable for 3D cell culture prepared by near-field electrospinning

Feng-Li He¹, Da-Wei Li¹, Jin He, Yang-Yang Liu, Fiaz Ahmad, Ya-Li Liu, Xudong Deng, Ya-Jing Ye*, Da-Chuan Yin*

Institute for Special Environmental Biophysics, Key Laboratory for Space Bioscience and Biotechnology, School of Life Sciences, Northwestern Polytechnical University, Xi'an 710072, PR China



ARTICLE INFO

Keywords:

Near-field electrospinning
Layer-structured scaffold
Osteogenic differentiation
Tissue engineering
Cell infiltration

ABSTRACT

Electrospinning is a powerful method for preparing porous materials that can be applied as biomedical materials for implantation or tissue engineering or as scaffolds for 3D cell culture experiments. However, this technique is limited in practical applications because the pore size of 3D scaffolds directly prepared by conventional electrospinning is usually less than several tens of micrometres, which may not be suitable for 3D cell culture and tissue growth. To allow for satisfactory 3D cell culture and tissue engineering, the pore size of the scaffold should be controllable according to the requirement of the specific cells to be cultured. Here, we show that layer-structured scaffolds with pore sizes larger than 100 µm can be obtained by stacking meshes prepared by direct-writing using the near-field electrospinning (NFES) technique. In the study, we prepared composite scaffolds made of polycaprolactone (PCL) and hydroxyapatite (HAp) via the above-mentioned method and tested the effectiveness of the novel scaffold in cell culture using mouse pre-osteoblast cells (MC3T3-E1). The pore size and the degradability of the PCL/HAp scaffolds were characterized. The results showed that the average pore size of the scaffolds was 167 µm, which was controllable based on the required application; the degradation rate was controllable depending on the ratio of PCL to HA. The biocompatibility of the scaffolds in vitro was studied, and it was found that the scaffolds showed no toxicity and that the cells could effectively attach, proliferate, and differentiate in the 3D skeleton of the scaffolds. Our studies showed that a simple modification of the preparation procedure can lead to a new way to fabricate novel layer-structured 3D scaffolds with controllable structures and pore sizes suitable for practical applications in implantation, tissue engineering and 3D cell culture.

1. Introduction

Three-dimensional (3D) scaffolds are critically important in the applications such as biomedical implantation, tissue engineering, and 3D cell culture. To be useful, the 3D scaffold should possess properties that can meet the specific requirements of different various applications. The properties of the scaffold that should be considered include morphology (porosity, pore size, and interconnectivity), mechanical properties, and biocompatibility. The properties of the 3D scaffold are determined by the preparation technique. Therefore, exploration and optimization of preparation techniques are necessary for obtaining suitable 3D scaffolds for practical utilization.

3D scaffolds are usually required to be porous. Many techniques that can generate porous materials have been studied extensively, such as, self-assembly [1], freeze-drying [2], 3D-printing [3,4], electrospinning [5,6], electrodeposition [7], sintering [8], etc. Among them,

electrospinning has demonstrated a great potential in biomedical applications [9,10]. Electrospun scaffolds exhibit significant advantages including a similar structure to the extracellular matrix (ECM), a large surface-to-volume ratio, and the ability to guide cells to attach and proliferate on the surface of the scaffold [11]. These advantages make the electrospun scaffold potentially useful as a competitive candidate for cell culture. However, use of electrospun scaffolds is often limited because the pore sizes of the scaffolds do not meet the requirement for cell culture or tissue engineering. To guarantee desirable cell infiltration and growth inside scaffolds, the pore size should be sufficiently large depended the types of cells. For bone tissue engineering, the minimum pore size requirement should be approximately 100 µm due to cell size, migration requirements and transport [12].

To overcome the difficulties, there have been some efforts to increase the pore size of electrospun scaffolds. One way to increase the pore size is co-electrospinning the target fibers together with sacrificial

* Corresponding authors.

E-mail addresses: yeajing@nwpu.edu.cn (Y.-J. Ye), yindc@nwpu.edu.cn (D.-C. Yin).

¹ These authors contributed equally to this work.

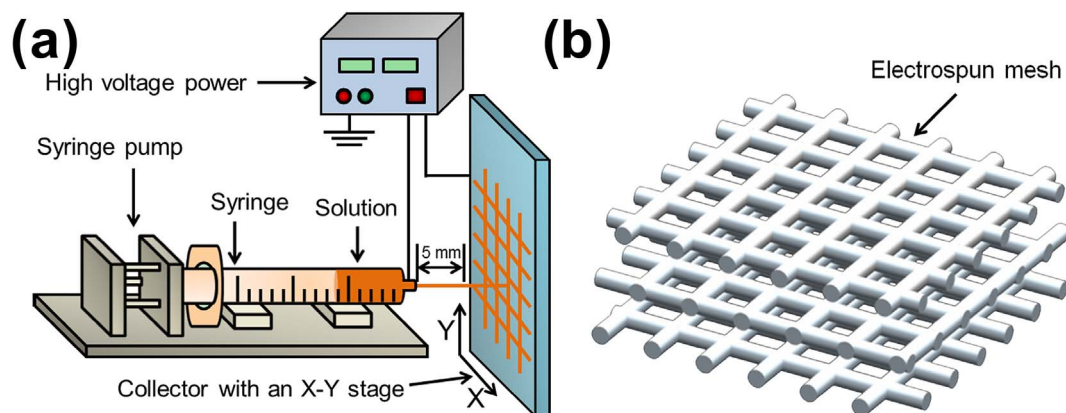


Fig. 1. Schematic illustration of the preparation of the 3D scaffolds. (a) Schematic diagram of direct-writing using the NFES technique. The distance between the syringe nozzle and collector was 5 mm. (b) Illustration of stacking the meshes layer-by-layer to form a 3D construct. After stacking, the 3D construct was heat-treated to yield the final 3D scaffold.

fibers that can be then be removed after the scaffold is prepared [13]. Similar methods such as salt-leaching [14], cryo-electrospinning [15] and limited protease digestion [16] have been studied, and encouraging results have been observed. Another way to increase the pore size is to adjust the collector so that the packing density of the scaffold can be tuned, leading to larger pore sizes that are controllable within a certain range [17,18]. Post-treatment after electrospinning is also a possible strategy. Ultrasonication [19] has been found to be useful in decreasing the packing density of the scaffold such that the pore size can be increased and, consequently, the cell infiltration can be enhanced. Although there have already been various approaches to achieve larger pore sizes in electrospun scaffolds, further enhancing the controllability of the structure and pore size is still urgently needed for applications in a large variety of situations.

In 2006, Sun et al. developed a near-field electrospinning (NFES) process to deposit single fiber in a direct, continuous, and controllable manner by reducing the applied voltage and the distance between needle and collector [20]. In this electrospinning process, the polymer was electrostatically drawn into a charged jet. After a short straight stable zone, the charged jet moved into a bending unstable zone, in which the charged jet was stretched and thinned. Finally, fibers were deposited randomly on the collector in a chaotic way. However, in the NFES process, the bending instability could be restricted by adjusting the speed of moving collector and reducing the distance between needle and collector. Therefore, the single fiber could be deposited with a good controllability in straight-line stage [21,22]. Due to its ability to control the deposition of single fiber, the NFES process had been widely applied in many fields, such as tissue engineering [23], wearable sensor [24] and energy storage [25]. Based on the NFES technology, here, we propose a new approach for preparing a layer-structured scaffold, the pore size of which is controllable over a wide range that may be suitable for purposes of cell culture and tissue engineering. The approach is simple: first, microfibrous meshes were prepared by direct-writing using NFES; second, the meshes were stacked layer-by-layer and fixed to form a 3D scaffold. The direct-writing process was controlled by a computer program; the size of the written grids could be controlled to any value over a large range greater several tens of micrometres. Stacking the meshes created 3D scaffold with the desired pore size largely determined by the size of the written grids.

To verify the effectiveness of this approach, we chose mouse pre-osteoblast cells (MC3T3-E1) for cell culture tests in the novel scaffold. PCL, a key polymer with high stability and excellent biocompatibility [26,27], was chosen as the primary material to prepare the scaffold. To overcome problem of cell adhesion, proliferation and migration [28] due to the hydrophobic nature of PCL, hydrophilic HA_p, as the main composition of the extracellular mineral phase, was chosen for mixing with the PCL such that the biocompatibility, osteo-conductivity and

bone bonding ability of the scaffold could be enhanced. The cell culture test using the novel scaffold showed encouraging results, confirming that the preparation method proposed in this work is potentially valuable and may represent a new route for fabrication of 3D scaffolds with controllable structure and pore size.

2. Materials and methods

2.1. Materials

PCL pellets ($M_n = 80000$ g/mol) were purchased from Sigma-Aldrich. 1,1,1,3,3-hexafluoro-2-propanol (HFIP) was obtained from Shanghai Conservation Chemical Technology Co., Ltd. HA_p particles were bought from Nanjing Emperor Nano Material Co., Ltd. Alpha-MEM modification (α -MEM) was bought from HyClone-Thermo Scientific. Foetal bovine serum (FBS) was obtained from Gibco-Invitrogen. Ascorbic acid and β -glycerophosphate were purchased from Sigma-Aldrich. TransZol™ Up was purchased from Trans Gen Biotech Co., Ltd.

2.2. Scaffold fabrication

A certain amount of HA_p particles and 1.5 g PCL pellets were added to 10 mL HFIP. The mixture was obtained at a series of weight ratios ($W_{HAp}: W_{PCL} = 3:7, 4:6, 5:5$). Then, the mixture was magnetically stirred at room temperature for 4 h until the mixture was homogeneous. In an electrospinning machine (SS-2553, Ucalerv, Beijing, China), the solutions were loaded into a 10-mL syringe with a 19-G blunt needle; the flow rate was 0.4 mm/min, and the applied high voltage was 3 kV, and the distance between the syringe nozzle and the grounded collector was 5 mm. The collector was attached to an X-Y stage controlled by a motion controller allowing the collector to be moved under control of a computer program. During the electrospinning process, the controller could drive the collector movement (3 m/min) along a predefined path. By using the direct writing method, fiber mesh ruled with vertical and horizontal lines could be obtained. The space between adjacent fibers is controllable. In this work, it was controlled to be 1 mm. Fig. 1(a) schematically shows direct-writing using the NFES technique. To obtain a 3D construct, 10 meshes were stacked layer-by-layer as shown in Fig. 1(b). Finally, the 3D constructs were heat-treated at 50 °C for 10 s to connect the layers to improve the structural integrity.

2.3. Scaffold characterization

The morphology and composition of the PCL/HA_p scaffolds were investigated using a scanning electron microscopy (SEM) coupled with energy-dispersive X-ray spectroscopy (EDS) (VEGA 3 LMU, TESCAN, Czech).

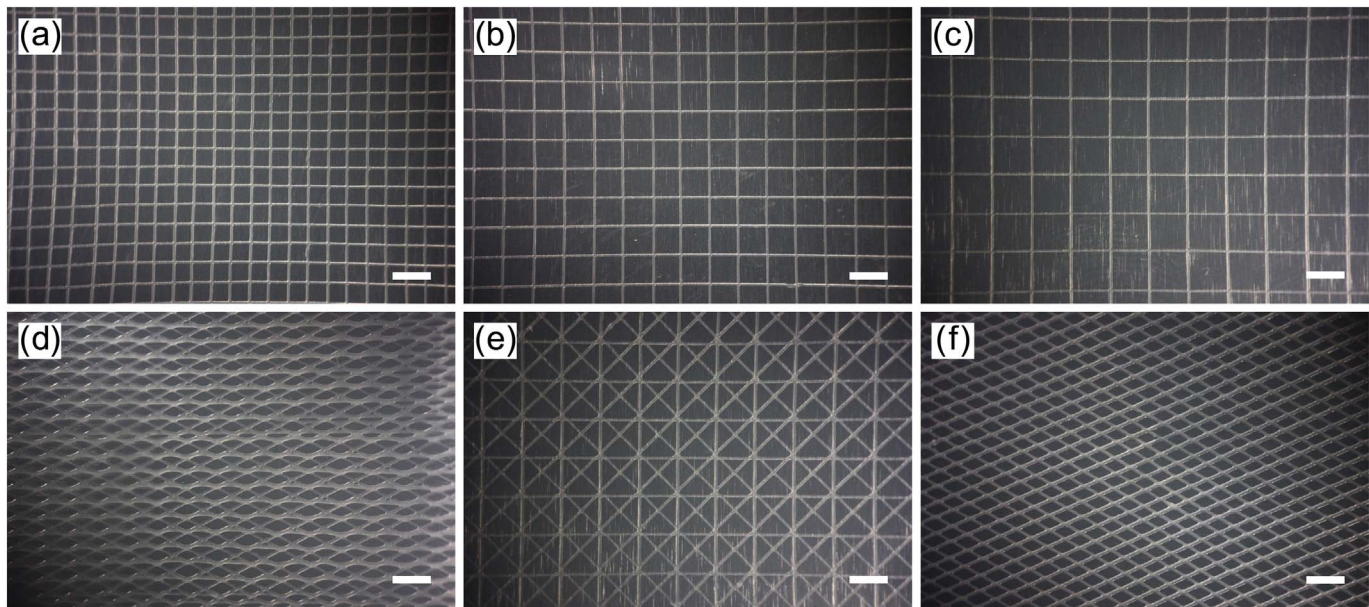


Fig. 2. The photographs of fiber meshes with different sizes and different structures. (a)–(c) The grid fiber meshes with controlled spacing of 1 mm, 1.5 mm and 2 mm, respectively; (d) and (e) the fiber meshes consist of triangles; (f) the fiber mesh consists of diamonds. Scale bar = 2 mm.

The phases of the composite scaffolds were characterized by a D/max-500 X-ray diffractometer (XRD) (Rigaku, Japan) equipped with a copper anticathode tube using a Cu anode at 40 kV and 200 mA in the 2θ range of 10° to 70° with steps of 0.02°.

Chemical components of the PCL/HAp composite scaffolds were studied by using a fourier transform infrared (FTIR) spectrometer (TENSOR27, Bruker, Germany) over a range of 4500 to 500 cm^{-1} at a resolution of 2 cm^{-1} averaging 100 scans.

The surface wettability of the scaffolds was characterized by measuring the contact angle of water on the surface of the scaffolds. 5 mL deionized water was pipetted onto the horizontal surface of the scaffolds. The contact angle was then obtained according to the droplet images.

The water absorption rates were calculated according to the following equation:

$$R_a(\%) = \frac{W_s - W_0}{W_0} * 100\% \quad (1)$$

Where R_a is the water absorption rate, and W_0 and W_s denote the weights of sample before and after immersion in distilled water for 1 h, respectively.

2.4. Biocompatibility characterization

After seeding the cells on the scaffolds 3 days, the cell-scaffold composites were fixed in 2.5% glutaraldehyde solution and then dehydrated successively in a concentration gradient of ethanol solutions. The cells morphology was observed using a Zeiss Super 55 scanning electron microscope (Zeiss, Germany).

After culturing for 1, 7, 14 and 21 days, cellular proliferation was quantified by using the MTT-based colorimetric assay as per the manufacturer's instructions.

For osteogenic differentiation, the culture medium was supplemented with 1 M β -glycerophosphate and 5 mg/mL ascorbic acid. The mRNA expression of osteogenic marker gene was analysed by RT-PCR. The total RNA was isolated by using a *TransZol™* Up kit after culturing for 3 days, 7 days, 11 days and 14 days. Single-strand cDNA was obtained by reverse transcription using 1 μg total RNA. PCR amplification of the cDNA was carried out by using a CFX96 Touch™ Real-Time PCR detection system.

To examine the host response to the PCL/HAp composite scaffolds, the scaffolds were implanted into the abdomens of rats. The rats were sacrificed at 28 days after surgery. The scaffolds with adjacent tissue were excised, fixed, embedded, sectioned, stained with haematoxylin and eosin (H&E) and analysed using a Nikon Eclipse-ci microscope (Eclipse-ci, Nikon, Japan).

2.5. Biodegradation *in vitro*

After immersed for 7, 14, 21 and 28 days, the mass loss ratio was calculated according to the following equation:

$$R_m(\%) = \frac{W_0 - W_s}{W_s} * 100\% \quad (2)$$

Where R_m represents the mass loss ratio, and W_0 and W_s denote the weights of scaffold before and after degradation test, respectively. The PBS in the wells was moved into a drying oven to volatilize the water, added into 3 mL 1% HNO_3 , and then the calcium concentration was measured by atomic absorption spectrometer (ZEENIT700P, Analytikjena, Germany).

3. Results and discussions

3.1. Characterization of the scaffolds (controllable morphology, stable phases, and improved wettability)

Near-field electrospinning in a direct-writing way is a novel technology to deposit orderly single fibers with a pre-designed trajectory. The fiber meshes with controllable size and structure could be fabricated by this technology. To demonstrate the controllability of this technology, a variety of single fiber meshes with controlled sizes and structures were deposited on aluminium foils by near-field electrospinning in a direct-writing way. As shown in Fig. 2, the fibers were smooth and straight, and there was no fusion phenomenon occurred at the fiber junctions. In addition, the well-defined structures were achieved by properly matching the collector speed with the jet speed. Furthermore, the size and structure of the single fiber meshes could be well controlled to satisfy different requirements.

For the 3D cell culture, a layer-structured scaffold was fabricated by stacking those fiber meshes with well-defined and controllable

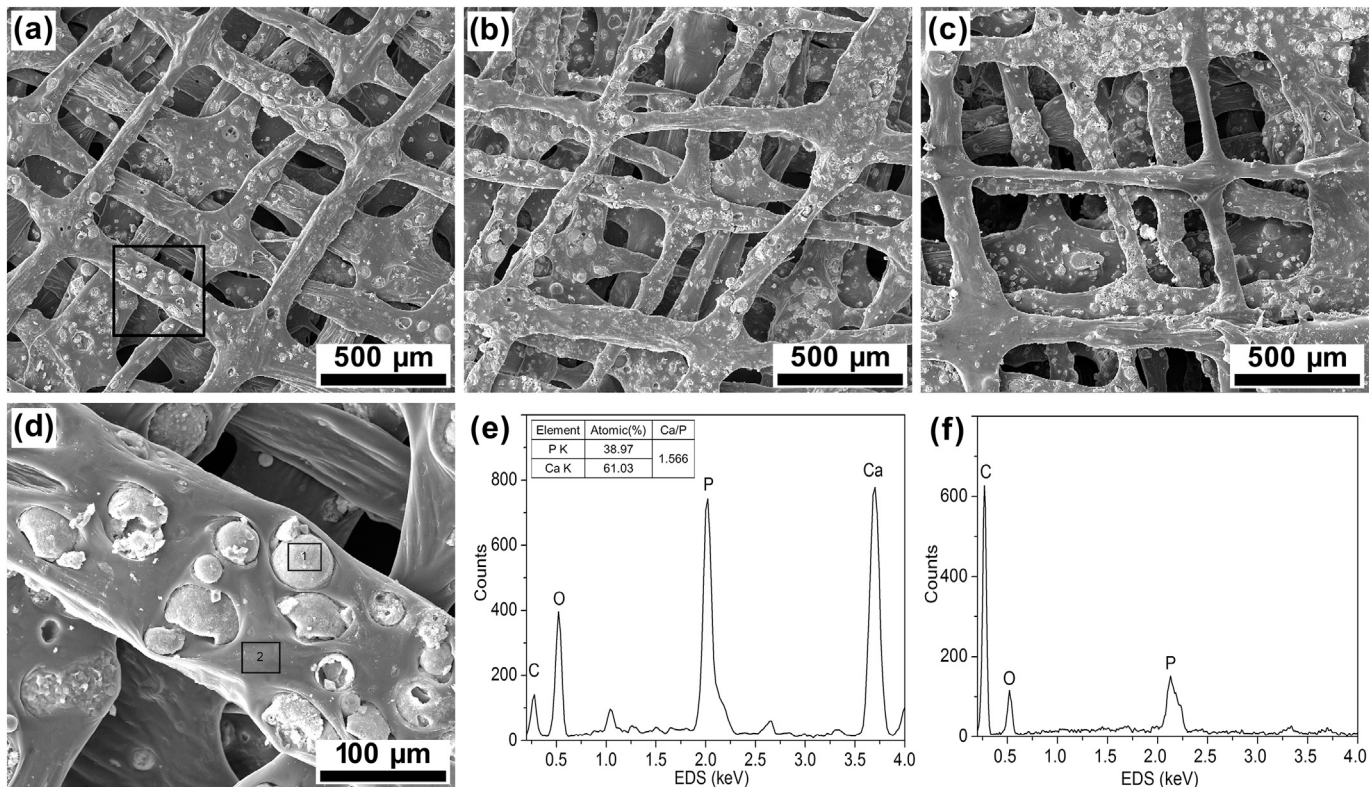


Fig. 3. Morphological characterization of the PCL/HAp composite scaffolds. (a)–(c): SEM image of PCL/0.3HAp scaffold, PCL/0.4HAp scaffold and PCL/0.5HAp scaffold; (d): high magnification of the square area in (a); (e): EDS spectrum of the particle (“1” in (d)); (f): EDS spectrum of the fiber (“2” in (d)).

Table 1
Diameters and pore sizes of PCL and PCL/HAp scaffolds.

Sample	Diameter (μm)	Pore size (μm)
PCL/0.3HAp	150.5 ± 41.2	159.3 ± 33.7
PCL/0.4HAp	108.3 ± 24.1	175.3 ± 40.4
PCL/0.5HAp	126.8 ± 22.1	168.1 ± 38.7

structures for many layers. As shown in Fig. 3, the layer-structured PCL/HAp scaffolds with an interconnected network structure were prepared; besides, the topologies of the scaffolds slightly varied with HAp content, showed in Fig. 3(a), (b) and (c). We also observed that the PCL/HAp composite scaffolds showed excellent connectivity, and no closed pores were observed. The average diameters and pore sizes of the composite PCL/HAp scaffolds were listed in Table 1. The results showed that, with increased HAp content from 30% to 40%, the average diameter of the fibers decreased from $150.5 \pm 41.2 \mu\text{m}$ to $108.3 \pm 24.1 \mu\text{m}$ and the pore size slightly increased from $159.3 \pm 33.7 \mu\text{m}$ to $175.3 \pm 40.4 \mu\text{m}$. Further increase of HAp content to 50% has very mild effect on the diameter of fiber and pore size. Due to the present of calcium and phosphate ions in HAp, the conductivity of the PCL/HAp solution increased [29]. With the conductivity increasing, the tensile force acting on the fiber increased, which lead to the diameter decreased. In addition, higher HAp content will lead to higher viscosity of PCL/HAp solution, which results in an increase in the diameter of fiber [30,31]. Since the distance between the centers of two adjacent fibers was fixed at 1 mm in our study, when the diameter of fiber increased, the pore size, namely the vacant spacing between fibers, would resultantly decrease. We examined the element components in both the fibers and the particles by EDS. Fig. 3(d) shows the tested positions, and Fig. 3(e) and (f) show the EDS spectra of the particles and fibers, respectively. Sharp peaks for P and Ca can be observed in Fig. 3(e), and the ratio of Ca/P was 1.566, which was close to

the theoretical ratio of 1.67 for HAp, suggesting that the main components of the particles were HAp. Similarly, the weak peaks of C and O shown in Fig. 3(f) were the essential elements of PCL, suggesting that, considering the chemicals used during the preparation process, the fibers were mainly PCL.

The layer-structured scaffolds with excellent connectivity and free of closed pores would promote cell culture. Furthermore, the controllable pore size provides a friendly environment for versatile purposes of growing different types of cells with satisfactory infiltration. The pore size of the scaffolds was determined mainly by the pattern prepared by direct-writing. However, the HAp content affect the pore size to some extent due to the effect of HAp content on the fiber diameter. Thus, in designing the pattern size, the HAp content should be considered. In this experiment, we controlled the pore size about $167 \mu\text{m}$, which is suitable for osteoblasts to infiltrate and grow into the scaffolds and convenient for the transport of nutrients and metabolic waste [32].

The crystalline state of PCL pellets, PCL/HAp scaffolds and HAp particles were examined and showed in Fig. 4(a). The sharp characteristic peaks of HAp particles were observed at 25.8° (002) and 31.5° (211). Additionally, weak characteristic peaks of HAp were also observed in three PCL/HAp scaffolds (Fig. 4(a)), which indicated that the HAp particles dispersed well in the fibers of the scaffolds and did not just appear on the surface of fibers [33]. Similarly, the characteristic peaks of the PCL at 21.3° (110) and a relatively weak peak at 23.6° (200) were appeared in the XRD patterns of all the PCL/HAp scaffolds, indicating that the scaffolds contained crystalline PCL. It should be noted that the diffraction peak intensity of PCL became weaker with increasing HAp content, suggesting that the PCL content in the composite scaffolds decreased.

The FTIR spectra of PCL, PCL/HAp scaffolds and HAp are shown in Fig. 4(b). The spectra of HAp showed strong and sharp peaks at 1050 cm^{-1} and 3430 cm^{-1} , which were assigned to the PO_3^{4-} groups and OH-ions of HAp, respectively. In the spectra of all the PCL/HAp

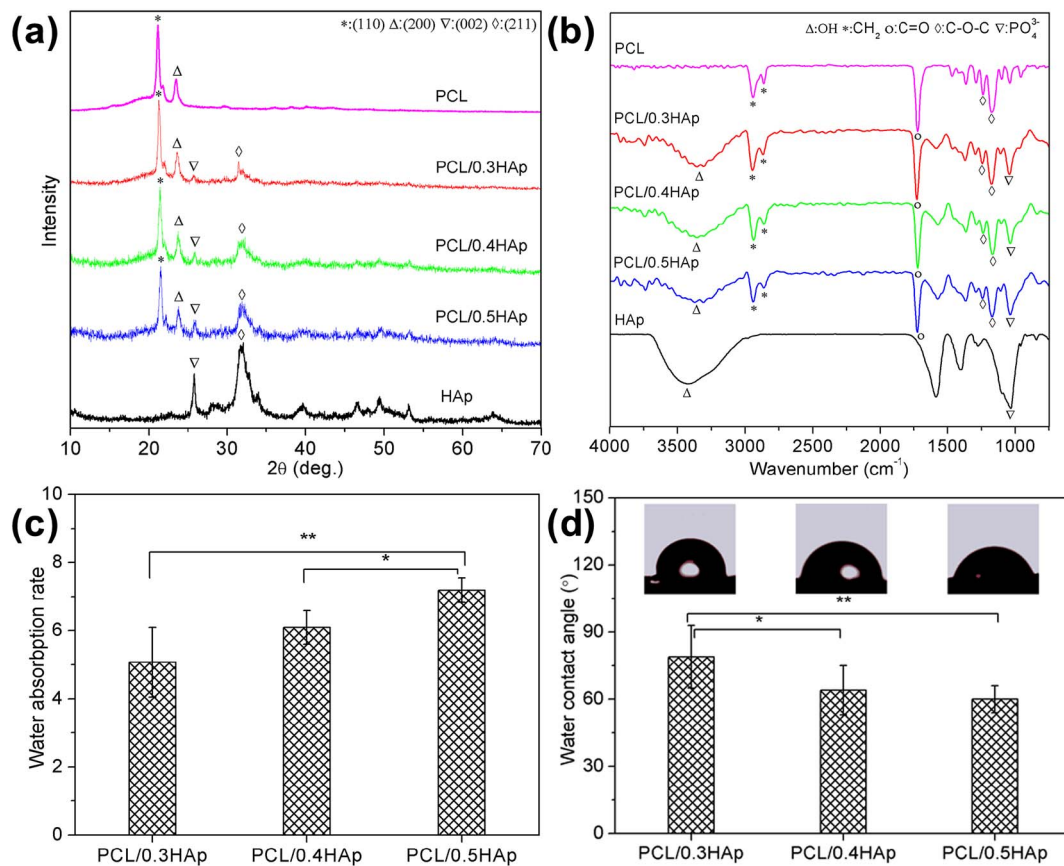


Fig. 4. Properties characterization of the PCL/HAp composite scaffolds. (a): X-ray diffraction pattern of PCL, PCL/HAp scaffolds and HAp; (b): fourier transform infrared spectra of PCL, PCL/HAp scaffolds and HAp; (c): the water absorption rate of the PCL/HAp scaffolds; (d): the water contact angle of the PCL/HAp scaffolds.

scaffolds, the same bands appeared, and no significant shifts were observed in the major absorption peaks, which were consistent with those of the original components. The HAp groups can absorb and band more serum proteins and growth factors, which is beneficial for the adhesion, differentiation and mineralization of osteoblasts [34]. The PCL spectrum showed the characteristic bands of C—O—C stretching vibration at 1176 cm⁻¹ and 1235 cm⁻¹, C=O stretching vibration at 1730 cm⁻¹, C—H asymmetric stretching vibration at 2939 cm⁻¹ and C—H symmetric stretching vibration at 2864 cm⁻¹. The existence of C—O—C and C=O cause PCL to exhibit a super hydrophobic property [35]. These characteristic bands of PCL could also be observed in the spectra of the PCL/HAp scaffolds.

To achieve satisfactory 3D cell culture, the surface of the scaffolds must be hydrophilic [36]. The water absorption rate of the scaffold can be used to show the surface wettability to some extent. Fig. 4(c) shows the water absorption rate of the PCL/HAp scaffolds. An increase in HAp content from 30% to 50% led to an increase in the water absorption rate of the PCL/HAp scaffolds from 5.07 to 7.18, suggesting that the water absorption rate was closely related to HAp content. Contact angle is another parameter that can be used to characterize surface properties. Fig. 4(d) shows the contact angle of water on the PCL/HAp scaffolds. When the HAp content increased from 30% to 50%, the contact angle decreased from 79 ± 14° to 60 ± 6°, indicating that the scaffolds showed better hydrophilicity at higher HAp contents. This result was in good agreement with the results of the water absorption test shown in Fig. 4(c). The main reason for this result may be that the hydrophilic functional groups (Ca²⁺, PO₃⁴, OH-ions) on the surface of HAp could bind H₂O molecules by hydrogen bonding and adsorption interactions, for instance, dipolar and dispersive interactions, with the HAp surface [37]. It was reported that a hydrophilic surface is better than a hydrophobic surface for cell attachment and growth because hydrophilic

surfaces can absorb more serum and growth factors from the medium, which contribute to improving the cell culture [38]. Our study verified that doping the scaffolds with HAp particles was use for improving or tuning the wettability of the scaffolds to avoid the drawbacks of PCL in cell culture.

3.2. Biocompatibility (promising for cell spreading, proliferation and differentiation; satisfactory behaviour after implantation)

In studies of the development of biomedical materials, biocompatibility is the primary aspect to be considered. The morphology of cells was observed by SEM images (see in Fig. 5(a)–(f)). Figs. 5(a) and (b) clearly show that the cells extended their cytoplasm and spread completely on the scaffolds. On the PCL/0.5HAp (Fig. 5(c)) scaffold, the cells almost reached confluence. At higher magnification, pseudopodia can be clearly observed. As shown in Fig. 5(d) and (e), lamellipodia appeared on the scaffolds, and in Fig. 5(f), filopodia can be found on the PCL/0.5HAp scaffold. The reason for this difference might be that the presence of HAp influenced cell signalling and responses [33]. The figures reveal that the pseudopodia of the cells could firmly connect with the fibers of the scaffolds and promote cell growth in three dimensions. This 3D growth behaviour of the cells in the scaffolds is similar to their *in vivo* behaviour.

Cell proliferation on the scaffolds was characterized by the MTT method. We used the variation of the MTT optical density (OD) value as an indicator of the cell proliferation. Fig. 5(g) showed that the cell proliferation on all PCL/HAp scaffolds significantly increased with the culture time each week ($P < 0.01$). From day 1 to day 7, the cell proliferation on the PCL/0.3HAp scaffold increased sharply, which was significantly higher than that of cells on the PCL/0.4HAp and the PCL/0.5HAp scaffolds (both $P < 0.05$). In the second week, the cell

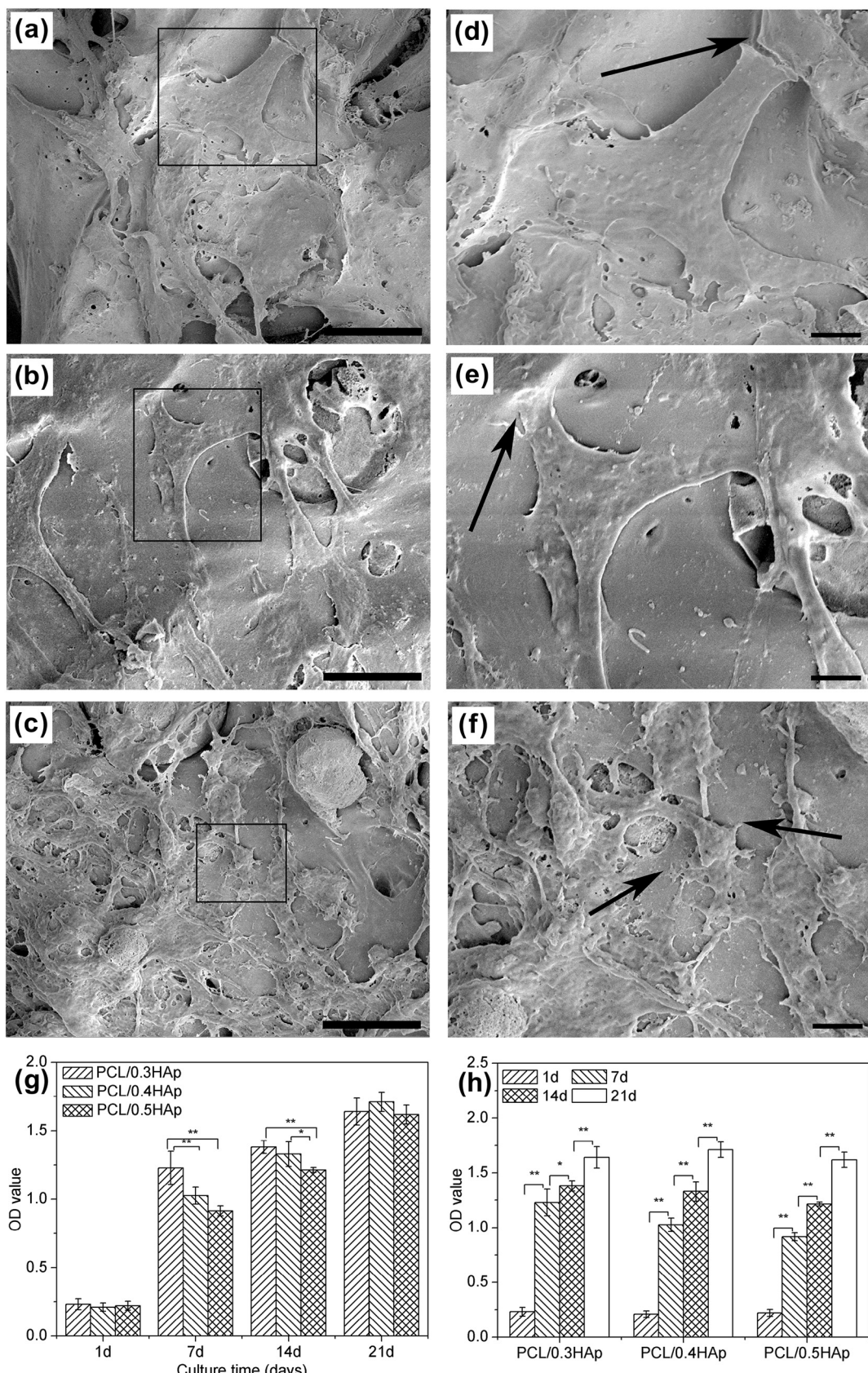


Fig. 5. The cells behaviours on the scaffolds. SEM images of cell morphologies on the scaffolds: (a) the PCL/0.3HAp scaffold, (b) the PCL/0.4HAp scaffold, (c) the PCL/0.5HAp scaffold. Bar = 20 μm . The arrows indicated the pseudopodia of the cells. (d), (e) and (f) are expansions of the insets in (a), (b) and (c), respectively. Scale bar = 5 μm ; (g) the OD value versus culture time; (h) the OD value versus HAp content.

proliferation on the PCL/0.5HAp scaffold was significantly slower than those on the other two scaffolds (both $P < 0.05$). However, in the third week, the cell proliferation on all of the scaffolds showed no significant differences. Based on these observations, the cell proliferation on the scaffold with lower HAp content was initially faster than that on scaffolds with higher HAp content; however, the trend gradually diminished when the culturing continued. We hypothesize that two or more controversial factors may affect the cell proliferation. On one hand, cell proliferation is correlated with the hydrophilicity of the scaffold [39,40]. When the hydrophilicity is high, cell attachment is facilitated, and thus, cell proliferation is promoted [39]. On the other hand, the presence of HAp particles in the scaffolds may influence cell signalling and thus affect the cell behaviours [33], which would result in suppressed growth of the cells [41]. The combination of the two factors may finally lead to the behaviours shown in Fig. 5(g). The cell proliferation differed for various HAp contents showed in Fig. 5(h). Notably, after the first week of culture, the cell proliferation on all scaffolds increased sharply. The increase in the OD value became slower in the following weeks. This result could be explained that the cells had enough space to proliferate in the first week, while in the following weeks, the proliferation became slower because of contact inhibition.

After culturing in the osteogenic medium for 3, 7, 11 and 15 days, the expression levels of osteogenic genes (ALP, OC, Runx2 and DMP1) of cells on the scaffolds were analysed by RT-PCR. Fig. 6(a) showed that the expression of ALP increased in the early stage of osteoblast differentiation and then decreased in the late stage. As an early marker of osteogenic differentiation, the expression of the ALP gene is expressed at high level in the early stage [42], ALP is necessary for cell mineralization by hydrolysing organic phosphate into inorganic phosphate, which was consistent with previous report that HAp could stimulate the precocious maturation of osteoblasts [41]. When the cells enter the mineralization stage, expression of the ALP gene is reduced [43]. As the late marker of cell differentiation, OC expression is very high in the mature bone cells [44]. In Fig. 6(b), the relative expression of OC gradually increased with culture time, suggesting that the cells in the

scaffolds gradually matured. When the cells entered the mineralization stage, the expression of OC reached its maximum. Runx2 is important for osteoblast differentiation and plays a regulatory role in osteoblast differentiation and bone formation processes. The expression of Runx2 is high in immature osteoblasts but low during osteoblast maturation [45]. Fig. 6(c) shows that the expression of Runx2 followed a similar trend, i.e., the expression of Runx2 remained at a higher level in the early stage and then gradually decreased. As a local factor, DMP1 plays a regulated role in bone mineralization [46], which indicates that high expression level of DMP1 always appears in the late stage of cell differentiation. Our observation confirmed that the expression of DMP1 increased in the late stage. In Fig. 6(d), the expression of DMP1 remained at a lower level in the beginning and then gradually increased, suggesting that the cells began to mineralize. As shown in Fig. 6, we also noticed that the gene expressions varied with different HAp contents. This result indicated that the present of HAp could induce the MC3T3-E1 cells to differentiate to osteoblast phenotype and could enhance the ECM formation and mineralization of pre-osteoblasts due to the apatite surface [32]. We therefore inferred that the appropriate HAp content can contribute to cell osteogenic differentiation [41].

The host response, which reflects the interaction between the materials and the body, is an important characteristic of biocompatibility. In this study, inflammatory reactions can generally be observed after surgical operations. The lymphocytes and macrophages are often found to be present at the site of inflammation and phagocytose foreign matter, then exit from the site of inflammation [47]. Hence, the presence of lymphocytes and macrophages indicates an inflammatory reaction. As shown in Fig. 7, a few lymphocytes and macrophages appeared at the location where the scaffold was implanted. Fig. 7(b) showed that the implanted scaffolds (labelled S) were encapsulated by newly formed connective tissue (labelled C). As shown in Fig. 7(c), a very limited number of lymphocytes (the white arrows) could be observed in the vicinity of the scaffold fibers. As shown in Fig. 7(a), there was a few macrophages (the white arrows) in the newly formed connective tissue. Based on the limited number of lymphocytes and

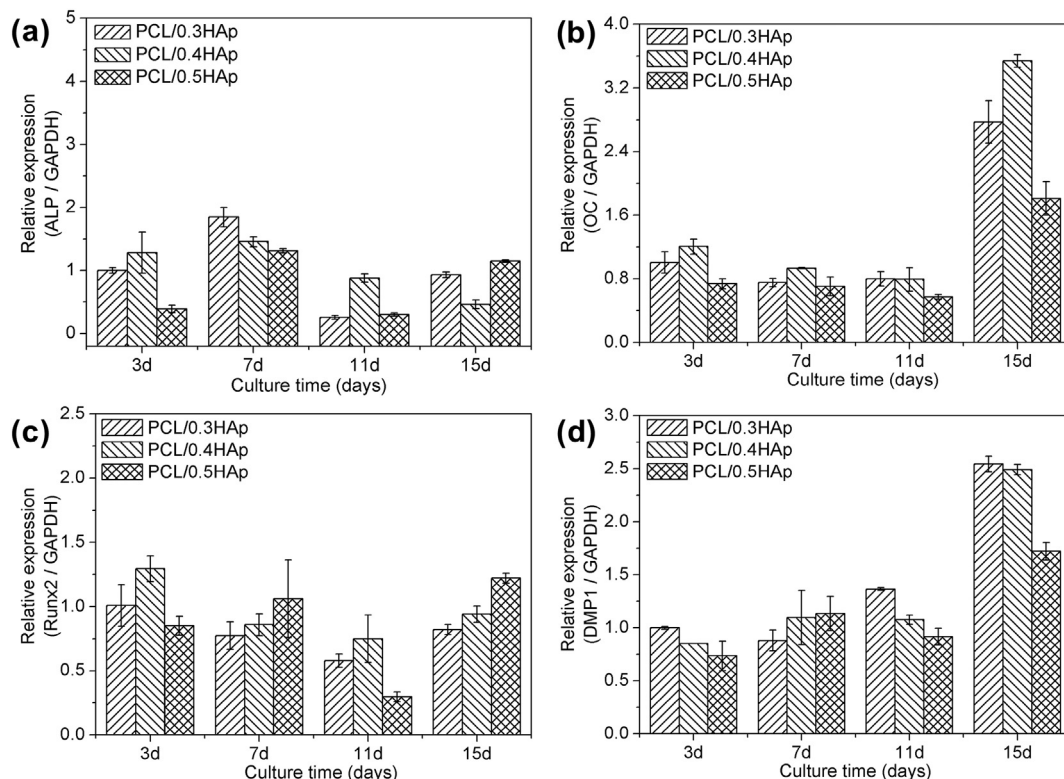


Fig. 6. The relative gene expression of the cells differentiated in osteogenic medium in PCL/HAp scaffolds for 3, 7, 11, and 15 days. (a): ALP, (b): OC, (c): Runx2, (d): DMP1.

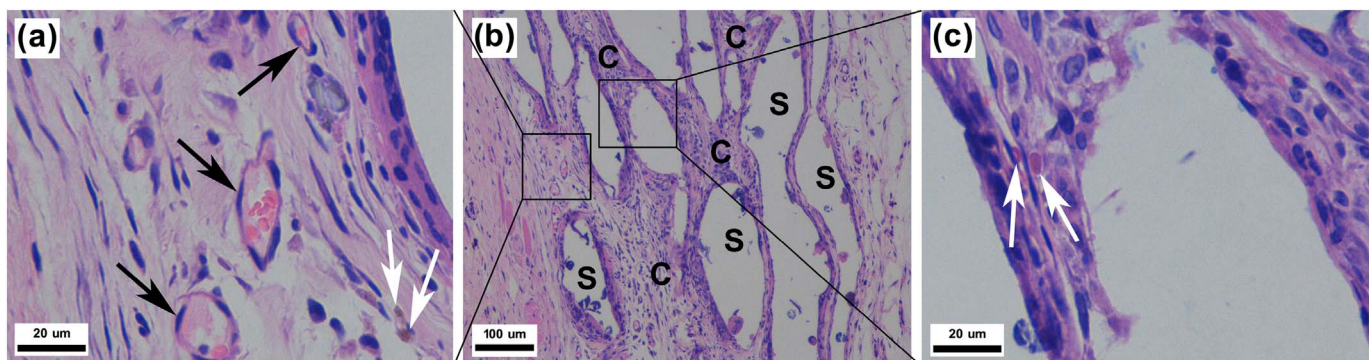


Fig. 7. Microscopic images of H&E-stained cross-sections of PCL/0.4HAp scaffolds with the adjacent tissue. (a): Expansion of the left inset in (b); (b): cross-section of a PCL/0.4HAp scaffold with the adjacent tissue; (c): expansion of the right inset in (b). C in (b) indicates new connective tissue filled into the gaps between scaffold fibers. S in (b) indicates the fibers of the PCL/0.4HAp scaffolds. The black arrows in (a) indicate the newly formed blood vessels contain blood cells. The white arrows in (c) indicate lymphocytes, and the white arrows in (a) indicate macrophages.

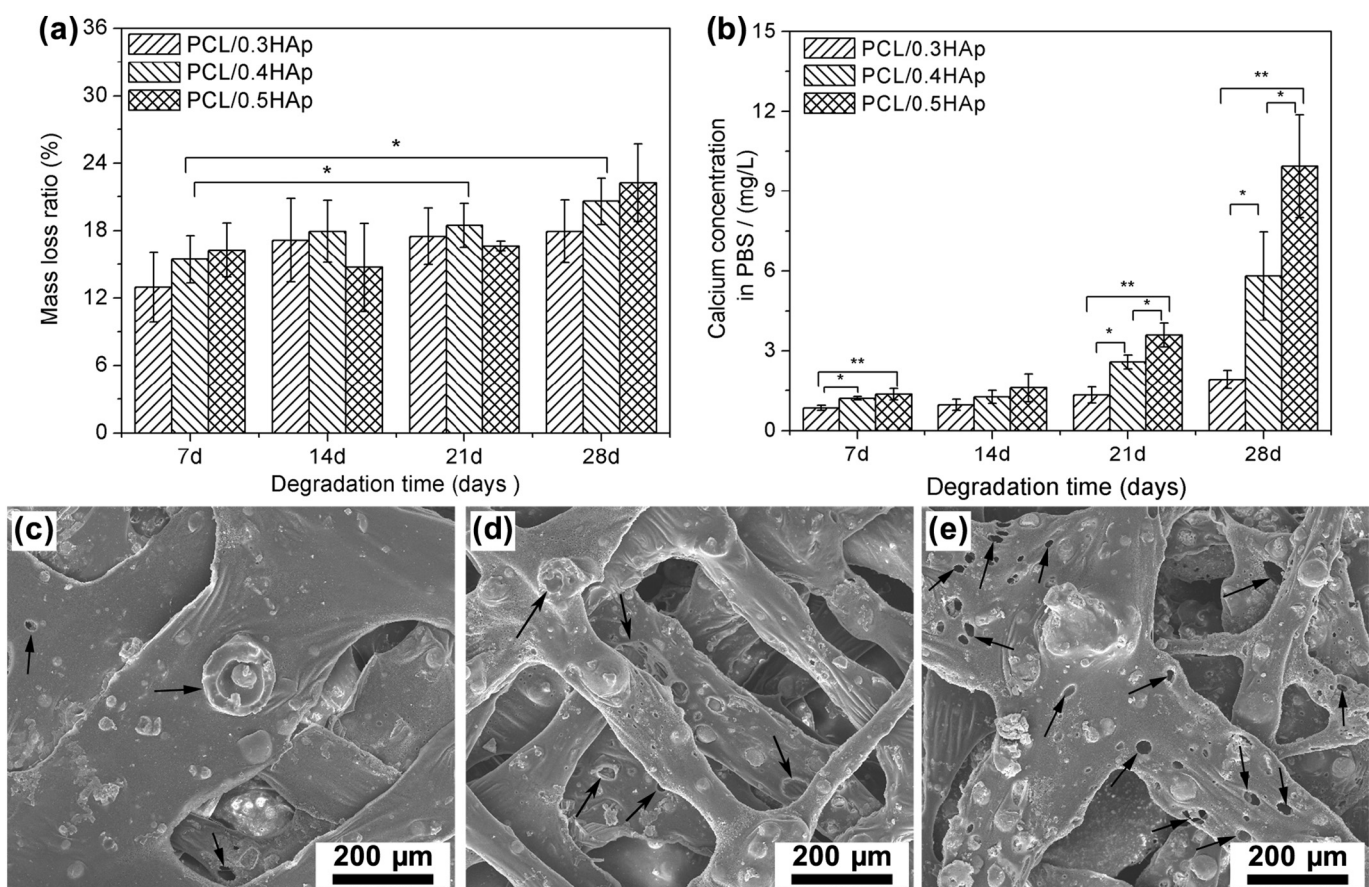


Fig. 8. Biodegradation behaviour of PCL/HAp scaffolds in vitro. (a) The mass loss ratio of the scaffolds after immersing; (b) the calcium concentrations in the PBS of the scaffolds after immersing; (c)–(e) SEM images of PCL/0.3HAp scaffolds, PCL/0.4HAp scaffold and PCL/0.5HAp scaffold after immersing in PBS for 28 day. Small voids (indicated by the arrows) can be observed in the images.

macrophages, we concluded that there was a slight chronic inflammatory reaction after implantation of the scaffolds into the bodies of the SD rats. It is worth mentioning that new blood vessels (indicated by black arrows in Fig. 7(a)) were prominent in the newly formed connective tissue. After transplantation, the surrounding tissue could grow into the inner scaffolds, and vascularization occurred at the interface between the scaffold and the surrounding tissue. The newly formed blood vessels, which could provide nourishment for the healing of bone fractures, play an important role in the repair and reconstruction of bone. Therefore, sufficient vascularization at damaged sites could improve bone formation during the bone tissue regeneration

[48].

These results proved that the PCL/HAp composite scaffolds we prepared demonstrated excellent biocompatibility both in vitro and in vivo. Moreover, we also found that the cell behaviours differed depending on different scaffolds with chemical composition of the scaffolds (e.g., HAp content), suggesting that the cell behaviour could be regulated by utilizing composite scaffolds with different structures and compositions.

3.3. Biodegradation (adjustable degradation)

Biodegradation is another important issue to be considered in the study and design of biomedical materials. Fig. 8(a) showed that the mass loss ratio of the PCL/HAp scaffolds increased with degradation time. Similarly, the calcium concentration in the PBS increased steadily with increasing degradation time (showed in Fig. 8(b)). A possible mechanism might be that some HAp particles detached from the fibers and entered the PBS solution, leaving voids on the scaffold. Thus, the integrity of the composite fibers could be compromised, which could accelerate PCL/HAp scaffold degradation. For the polymer PCL, the time needed for full degradation *in vivo* is approximately 1–2 years [49]. Therefore, it is impossible for PCL to completely degrade within just one month. According to the SEM images (Fig. 3), the HAp particles were embedded in the fibers. Hence, it can be proposed that the mass loss of the PCL/HAp scaffolds was caused by the reduced number of HAp particles in the fibers. The morphologies of the PCL/HAp scaffolds were investigated for 28 days to observe the degradation behaviour of the scaffolds. Fig. 8(c–e) shows the SEM images of the scaffolds were incubated in PBS solution for 28 days. The scaffolds clearly showed different degradation rates because of the different HAp contents. As shown in Fig. 8(c–e), there were many small voids in the fibers (indicated by the arrows), and higher HAp contents corresponded more voids. When the scaffolds were not immersed in PBS solution, small voids were rarely observed (Fig. 3). Comparison of the images confirmed that the mass loss may be mainly caused by the detachment of the HAp particles from the fibers. The composite scaffolds can exhibit adjustable degradation behaviour if the size and content of the HAp particles in the scaffold are properly controlled. This behaviour is essential for tissue repair because different tissues require scaffolds with different degradation rates.

3.4. Perspectives

The scaffold preparation method demonstrated here can be further modified to better suit different purposes. For instance, the method can be easily applied to prepare scaffolds with a gradient structure or designed structure, i.e., structures with a designed pore size distribution, to satisfy different requirements of cell culture or tissue engineering. To further enhance the applicability of the method proposed in this paper, the manual stacking process used in this method may be automated so that the stacking mode can be more strictly controlled and scaffold structures with different topologies and pore sizes can be more accurately realized.

4. Conclusion

In this study, we proposed a novel fabrication method to fabricate 3D scaffolds with controllable structures and pore sizes. The scaffolds exhibited excellent interconnectivity, and the average pore size of the scaffolds was approximately 167 μm , which was apparently controllable based on the application requirements. EDS, XRD and FTIR analyses showed that the chemical and phase properties of the PCL and HAp raw materials remained constant after the electrospinning process. The existence of HAp in the scaffolds enhanced the wettability of the scaffolds, promoted cell proliferation and differentiation, and allowed for the tuning of degradation properties. In the *in vitro* cell culture, we demonstrated that the cells could spread, proliferate and differentiate in the 3D scaffolds for an extended period of time. We concluded that the current results may open a new route for fabricating 3D scaffolds with controllable structures and pore sizes.

Acknowledgements

This work was supported by the National Natural Science Foundation of China (Grant No. U1632126), the Natural Science Basic

Research Plan in Shaanxi Province of China (Grant Nos. 2015JM5203, 2016JM3012), and the Fundamental Research Funds for the Central Universities (Grant Nos. 3102016ZY039, 3102015BJ(II)ZS011).

References

- [1] X.H. He, W. Wang, Y.M. Liu, M.Y. Jiang, F. Wu, K. Deng, Z. Liu, X.J. Ju, R. Xie, L.Y. Chu, Microfluidic fabrication of bio-inspired microfibers with controllable magnetic spindle-knots for 3D assembly and water collection, *ACS Appl. Mater. Interfaces* 7 (2015) 17471–17481, <http://dx.doi.org/10.1021/acsmami.5b05075>.
- [2] M. Ashokkumar, A.C. Chipara, N.T. Narayanan, A. Anumary, R. Sruthi, P. Thanikaivelan, R. Vajtai, S.A. Mani, P.M. Ajayan, Three-dimensional porous sponges from collagen biowastes, *ACS Appl. Mater. Interfaces* 8 (2016) 14836–14844, <http://dx.doi.org/10.1021/acsmami.6b04582>.
- [3] M.A. Nowicki, N.J. Castro, M.W. Plesniak, L.G. Zhang, 3D printing of novel osteochondral scaffolds with graded microstructure, *Nanotechnology* 27 (2016) 414001, <http://dx.doi.org/10.1088/0957-4448/27/41/414001>.
- [4] X. Zhou, N.J. Castro, W. Zhu, H.T. Cui, M. Aliaabouzar, K. Sarkar, L.G. Zhang, Improved human bone marrow mesenchymal stem cell osteogenesis in 3D bio-printed tissue scaffolds with low intensity pulsed ultrasound stimulation, *Sci. Rep.* 6 (2016) 32876.
- [5] D. Kai, M.P. Prabhakaran, B.Q.Y. Chan, S.S. Liow, S. Ramakrishna, F. Xu, X.J. Loh, Elastic poly(epsilon-caprolactone)-polydimethylsiloxane copolymer fibers with shape memory effect for bone tissue engineering, *Biomed. Mater.* 11 (2016), <http://dx.doi.org/10.1088/1748-6041/11/1/015007>.
- [6] J. Hu, D. Kai, H. Ye, L. Tian, X. Ding, S. Ramakrishna, X.J. Loh, Electrospinning of poly(glycerol sebacate)-based nanofibers for nerve tissue engineering, *Mater. Sci. Eng.*, C 70 (2017) 1089–1094, <http://dx.doi.org/10.1016/j.msec.2016.03.035>.
- [7] J. He, F.L. He, D.W. Li, Y.L. Liu, D.C. Yin, A novel porous Fe/Fe-W alloy scaffold with a double-layer structured skeleton preparation, *in vitro* degradability and biocompatibility, *Colloids Surf. B* 142 (2016) 325–333.
- [8] L. Zhang, Z.Y. He, Y.Q. Zhang, Y.H. Jiang, R. Zhou, Enhanced *in vitro* bioactivity of porous NiTi-HA composites with interconnected pore characteristics prepared by spark plasma sintering, *Mater. Des.* 101 (2016) 170–180, <http://dx.doi.org/10.1016/j.matdes.2016.03.128>.
- [9] R. Lakshminarayanan, R. Sridhar, X.J. Loh, M. Nandhakumar, V.A. Barathi, M. Kalaipriya, J.L. Kwan, S.P. Liu, R.W. Beuerman, S. Ramakrishna, Interaction of gelatin with polyenes modulates antifungal activity and biocompatibility of electrospun fiber mats, *Int. J. Nanomedicine* 9 (2014) 2439–2458, <http://dx.doi.org/10.2147/IJNN.S58487>.
- [10] X.J. Loh, P. Peh, S. Liao, C. Sng, J. Li, Controlled drug release from biodegradable thermo-responsive physical hydrogel nanofibers, *J. Control. Release* 143 (2010) 175–182, <http://dx.doi.org/10.1016/j.jconrel.2009.12.030>.
- [11] D. Kai, M.J. Tan, M.P. Prabhakaran, B.Q.Y. Chan, S.S. Liow, S. Ramakrishna, X.J. Loh, Biocompatible electrically conductive nanofibers from inorganic-organic shape memory polymers, *Colloids Surf. B* 148 (2016) 557–565.
- [12] V. Karageorgiou, D. Kaplan, Porosity of 3D biomaterial scaffolds and osteogenesis, *Biomaterials* 26 (2005) 5474–5491, <http://dx.doi.org/10.1016/j.biomaterials.2005.02.002>.
- [13] B.M. Baker, A.O. Gee, R.B. Metter, A.S. Nathan, R.A. Marklein, J.A. Burdick, R.L. Mauck, The potential to improve cell infiltration in composite fiber-aligned electrospun scaffolds by the selective removal of sacrificial fibers, *Biomaterials* 29 (2008) 2348–2358, <http://dx.doi.org/10.1016/j.biomaterials.2008.01.032>.
- [14] L.D. Wright, T. Andric, J.W. Freeman, Utilizing NaCl to increase the porosity of electrospun materials, *Mater. Sci. Eng.*, C 31 (2011) 30–36, <http://dx.doi.org/10.1016/j.msec.2010.02.001>.
- [15] M.F. Leong, K.S. Chian, P.S. Mhaisalkar, W.F. Ong, B.D. Ratner, Effect of electrospun poly(D,L-lactide) fibrous scaffold with nanoporous surface on attachment of porcine esophageal epithelial cells and protein adsorption, *J. Biomed. Mater. Res. A* 89A (2009) 1040–1048, <http://dx.doi.org/10.1002/jbm.a.32061>.
- [16] M.C. Phipps, W.C. Clem, J.M. Grunda, G.A. Cline, S.L. Bellis, Increasing the pore sizes of bone-mimetic electrospun scaffolds comprised of polycaprolactone, collagen I and hydroxyapatite to enhance cell infiltration, *Biomaterials* 33 (2012) 524–534, <http://dx.doi.org/10.1016/j.biomaterials.2011.09.080>.
- [17] K.P. Fuller, D. Gaspar, L.M. Delgado, A. Pandit, D.I. Zeugolis, Influence of porosity and pore shape on structural, mechanical and biological properties of poly epsilon-caprolactone electrospun fibrous scaffolds, *Nanomedicine* 11 (2016) 1031–1040, <http://dx.doi.org/10.2217/nmm.16.21>.
- [18] B.A. Blakeney, A. Tambralli, J.M. Anderson, A. Andukuri, D.-J. Lim, D.R. Dean, H.-W. Jun, Cell infiltration and growth in a low density, uncompressed three-dimensional electrospun nanofibrous scaffold, *Biomaterials* 32 (2011) 1583–1590, <http://dx.doi.org/10.1016/j.biomaterials.2010.10.056>.
- [19] J.B. Lee, S.I. Jeong, M.S. Bae, D.H. Yang, D.N. Heo, C.H. Kim, E. Alsberg, I.K. Kwon, Highly porous electrospun nanofibers enhanced by ultrasonication for improved cellular infiltration, *Tissue Eng. A* 17 (2011) 2695–2702, <http://dx.doi.org/10.1089/ten.tea.2010.0709>.
- [20] D.H. Sun, C. Chang, S. Li, L.W. Lin, Near-field electrospinning, *Nano Lett.* 6 (2006) 839–842, <http://dx.doi.org/10.1021/nl0602701>.
- [21] X.X. He, J. Zheng, G.F. Yu, M.H. You, M. Yu, X. Ning, Y.Z. Long, Near-field electrospinning: progress and applications, *J. Phys. Chem. C* 121 (2017) 8663–8678, <http://dx.doi.org/10.1021/acs.jpcc.6b12783>.
- [22] T.D. Brown, P.D. Dalton, D.W. Hutmacher, Direct writing by way of melt electrospinning, *Adv. Mater.* 23 (2011) 5651–5657, <http://dx.doi.org/10.1002/adma.201103482>.

- [23] P. Fattahi, J.T. Dover, J.L. Brown, 3D near-field electrospinning of biomaterial microfibers with potential for blended microfiber-cell-loaded gel composite structures, *Adv. Healthc. Mater.* (2017), <http://dx.doi.org/10.1002/adhm.201700456>.
- [24] Y.K. Fuh, Z.M. Huang, B.S. Wang, S.C. Li, Self-powered active sensor with concentric topography of piezoelectric fibers, *Nanoscale Res. Lett.* 12 (2017), <http://dx.doi.org/10.1186/s11671-016-1786-x>.
- [25] C. Shen, C.P. Wang, M. Sanghadasac, L. Lina, Flexible micro-supercapacitors prepared using direct-write nanofibers, *RSC Adv.* 7 (2017) 11724–11731, <http://dx.doi.org/10.1039/C6RA28218K>.
- [26] D. Kai, S. Jiang, Z.W. Low, X.J. Loh, Engineering highly stretchable lignin-based electrospun nanofibers for potential biomedical applications, *J. Mater. Chem. B* 3 (2015) 6194–6204, <http://dx.doi.org/10.1039/C5TB00765H>.
- [27] D. Kai, S.S. Liow, X.J. Loh, Biodegradable polymers for electrospinning: towards biomedical applications, *Mater. Sci. Eng., C* 45 (2014) 659–670, <http://dx.doi.org/10.1016/j.msec.2014.04.051>.
- [28] W.J. Li, J.A. Cooper Jr., R.L. Mauck, R.S. Tuan, Fabrication and characterization of six electrospun poly(alpha-hydroxy ester)-based fibrous scaffolds for tissue engineering applications, *Acta Biomater.* 2 (2006) 377–385, <http://dx.doi.org/10.1016/j.actbio.2006.02.005>.
- [29] V. Thomas, S. Jagani, K. Johnson, M.V. Jose, D.R. Dean, Y.K. Vohra, E. Nyairo, Electrospun bioactive nanocomposite scaffolds of polycaprolactone and nanohydroxyapatite for bone tissue engineering, *J. Nanosci. Nanotechnol.* 6 (2006) 487–493, <http://dx.doi.org/10.1166/jnn.2006.097>.
- [30] V. Thomas, D.R. Dean, M.V. Jose, B. Mathew, S. Chowdhury, Y.K. Vohra, Nanostructured biocomposite scaffolds based on collagen coelectrospun with nanohydroxyapatite, *Biomacromolecules* 8 (2007) 631–637, <http://dx.doi.org/10.1021/bm060879w>.
- [31] M.M. Li, W.W. Liu, J.S. Sun, Y.L. Xianyu, J.D. Wang, W. Zhang, W.F. Zheng, D.Y. Huang, S.Y. Di, Y.Z. Long, X.Y. Jiang, Culturing primary human osteoblasts on electrospun poly(lactic-co-glycolic acid) and poly(lactic-co-glycolic acid)/nanohydroxyapatite scaffolds for bone tissue engineering, *ACS Appl. Mater. Interfaces* 5 (2013) 5921–5926, <http://dx.doi.org/10.1021/am401937m>.
- [32] B.M. Whited, J.R. Whitney, M.C. Hofmann, Y. Xu, M.N. Rylander, Pre-osteoblast infiltration and differentiation in highly porous apatite-coated PLLA electrospun scaffolds, *Biomaterials* 32 (2011) 2294–2304, <http://dx.doi.org/10.1016/j.biomaterials.2010.12.003>.
- [33] D. Cao, Y.P. Wu, Z.F. Fu, Y. Tian, C.J. Li, C.Y. Gao, Z.L. Chen, X.Z. Feng, Cell adhesive and growth behavior on electrospun nanofibrous scaffolds by designed multifunctional composites, *Colloids Surf. B* 84 (2011) 26–34.
- [34] L.H. Lao, Y.J. Wang, Y. Zhu, Y.Y. Zhang, C.Y. Gao, Poly(lactide-co-glycolide)/hydroxyapatite nanofibrous scaffolds fabricated by electrospinning for bone tissue engineering, *J. Mater. Sci. Mater. Med.* 22 (2011) 1873–1884, <http://dx.doi.org/10.1007/s10856-011-4374-8>.
- [35] T.H. Nguyen, A.R. Padallin, H.S. Seo, B.T. Lee, A hybrid electrospun PU/PCL scaffold satisfied the requirements of blood vessel prosthesis in terms of mechanical properties, pore size, and biocompatibility, *J. Biomater. Sci. Polym. Ed.* 24 (2013) 1692–1706, <http://dx.doi.org/10.1080/09205063.2013.792642>.
- [36] M.T. Khorasani, H. Mirzadeh, S. Irani, Plasma surface modification of poly (l-lactic acid) and poly (lactic-co-glycolic acid) films for improvement of nerve cells adhesion, *Radiat. Phys. Chem.* 77 (2008) 280–287, <http://dx.doi.org/10.1016/j.radphyschem.2007.05.013>.
- [37] A. Dabrowski, V.A. Tertykh, Adsorption on New and Modified Inorganic Sorbents, Elsevier, 1996.
- [38] S.R. Son, R.A. Franco, S.H. Bae, Y.K. Min, B.T. Lee, Electrospun PLGA/gelatin fibrous tubes for the application of biodegradable intestinal stent in rat model, *J. Biomed. Mater. Res., Part B* 101 (2013) 1095–1105.
- [39] B. Chuenjittukuntaworn, W. Inrung, D. Damrongsi, K. Mekaapiruk, P. Supaphol, P. Pavasant, Polycaprolactone/hydroxyapatite composite scaffolds: preparation, characterization, and in vitro and in vivo biological responses of human primary bone cells, *J. Biomed. Mater. Res. A* 94A (2010) 241–251, <http://dx.doi.org/10.1002/jbma.a.32657>.
- [40] L.C. Xu, C.A. Siedlecka, Effects of surface wettability and contact time on protein adhesion to biomaterial surfaces, *Biomaterials* 28 (2007) 3273–3283, <http://dx.doi.org/10.1016/j.biomaterials.2007.03.032>.
- [41] R. Shu, R. McMullen, M.J. McCabe, Hydroxyapatite accelerates differentiation and suppresses growth of MC3T3-E1 osteoblasts, *J. Biomed. Mater. Res. A* 67A (2003) 1196–1204, <http://dx.doi.org/10.1002/jbma.20021>.
- [42] D. Kai, M.P. Prabhakaran, B.Q.Y. Chan, S.S. Liow, S. Ramakrishna, F. Xu, X.J. Loh, Engineering poly(lactide)-lignin nanofibers with antioxidant activity for biomedical application, *ACS Sustain. Chem. Eng.* 4 (2016) 5268–5276, <http://dx.doi.org/10.1021/acssuschemeng.6b00478>.
- [43] L.T. Nguyen, S. Liao, C.K. Chan, S. Ramakrishna, Enhanced osteogenic differentiation with 3D electrospun nanofibrous scaffolds, *Nanomedicine* 7 (2012) 1561–1575, <http://dx.doi.org/10.2217/nmn.12.41>.
- [44] A.L. Boskey, Matrix proteins and mineralization: an overview, *Connect. Tissue Res.* 35 (1996) 357–363.
- [45] Z. Maruyama, C.A. Yoshida, T. Furuchi, N. Amizuka, M. Ito, R. Fukuyama, T. Miyazaki, H. Kitaura, K. Nakamura, T. Fujita, N. Kanatani, T. Moriishi, K. Yamana, W. Liu, H. Kawaguchi, K. Nakamura, T. Komori, Runx2 determines bone maturity and turnover rate in postnatal bone development and is involved in bone loss in estrogen deficiency, *Dev. Dyn.* 236 (2007) 1876–1890, <http://dx.doi.org/10.1002/dvdy.21187>.
- [46] J.W. Lee, A. Yamaguchi, T. Iimura, Functional heterogeneity of osteocytes in FGF23 production: the possible involvement of DMP1 as a direct negative regulator, *BoneKey Rep.* 3 (2014) 543, <http://dx.doi.org/10.1038/bonekey.2014.38>.
- [47] S.F. Badylak, T.W. Gilbert, Immune response to biologic scaffold materials, *Semin. Immunol.* 20 (2008) 109–116, <http://dx.doi.org/10.1016/j.smim.2007.11.003>.
- [48] Y. Kang, L. Ren, Y. Yang, Engineering vascularized bone grafts by integrating a biomimetic periosteum and beta-TCP scaffold, *ACS Appl. Mater. Interfaces* 6 (2014) 9622–9633, <http://dx.doi.org/10.1021/am502056q>.
- [49] K. Rezwan, Q.Z. Chen, J.J. Blaker, A.R. Boccaccini, Biodegradable and bioactive porous polymer/inorganic composite scaffolds for bone tissue engineering, *Biomaterials* 27 (2006) 3413–3431, <http://dx.doi.org/10.1016/j.biomaterials.2006.01.039>.